Roh et al. Nanoscale Research Letters (2017) 12:353
DOI 10.1186/s11671-017-2126-5

Nanoscale Research Letters

NANO EXPRESS Open Access

Ferroelectric domain states of a tetragonal $BiFeO_3$ thin film investigated by second harmonic generation microscopy

Chang Jae Roh[1], Sun Young Hamh[1], Chang-Soo Woo[2], Kwang-Eun Kim[2], Chan-Ho Yang[2] and Jong Seok Lee[1*]

Abstract

We investigate the ferroelectric state of a tetragonal $BiFeO_3$ thin film grown on a $LaAlO_3$ (001) substrate using an optical second harmonic generation (SHG) microscope. Whereas the ferroelectric state of this material hosts nanometer-sized domains which again form micrometer-sized domains of four different configurations, we could figure out the characteristic features of each domain from the SHG mapping with various sizes of the probe beam, i.e., from 0.7 to 3.9 μm in its diameter. In particular, we demonstrate that a single micrometer-sized domain contributes to the SHG as a coherent summation of the constituent nanometer-sized domains, and multi-micrometer-sized domains contribute to the SHG as an incoherent summation of each micro-domain.

Keywords: Ferroelectrics, $BiFeO_3$, Thin film, Second harmonic generation, Multi-domain

PACS: 77.84.-s, 77.55.Nv, 78.20.-e

Background

Ferroelectrics have a great importance in both fundamental research and technical applications. Among them, $BiFeO_3$ (BFO) has attracted a large attention since it hosts, as a multiferroic material, both ferroelectric and antiferromagnetic properties at the same time; it undergoes a ferroelectric phase transition at 1103 K and antiferromagnetic phase transition at 643 K [1–3]. In particular, it exhibits a large magnetoelectric effect even at room temperature [3–5] and can be used for novel functional devices, for example, in a multi-storage information technology. As in other ferroelectric materials, BFO is known to have several types of ferroelectric domains with a size ranging from nanometer to micrometer scale [6, 7]. Such a local ferroelectric domain distribution and the characteristics of individual domains have been characterized often by using piezoresponse force microscopy (PFM) with controls of temperature, electric field, and crystal strain, which revealed several intriguing phenomena, such as conducting domain wall, flexoelectric effect, and morphotropic phase boundaries [8–10].

As an alternative technique to investigate the ferroelectric properties, an optical second harmonic generation (SHG) also has been widely adopted [11–14]. The ferroelectric state with no inversion symmetry usually provides strong second harmonic signals which show specific anisotropic patterns depending on the symmetry of the material. As a non-contact optical method, this technique can be usefully exploited in the characterization of ferroelectric or polar systems with a large leakage current. Since the SHG process is allowed only when the spatial inversion symmetry is broken, it has been used also to examine the symmetry lowering at the (sub)nanometer-scale surface or interfacial state of centrosymmetric bulk or thin films [15]. Furthermore, the nanometer-scale domain distribution has been successfully demonstrated by using the SHG technique combined with a scanning probe microscope [16]. Nevertheless, it is usually difficult to investigate the individual domains by using the conventional SHG microscope as the spatial resolution is limited by a fundamental diffraction which is about several hundred nanometers in the visible spectral range [17]. SHG studies on $BiFeO_3$ have been performed by several research

* Correspondence: jsl@gist.ac.kr
[1]Department of Physics and Photon Science, Gwangju Institute of Science and Technology (GIST), 123 Cheomdangwagi-ro, Buk-gu, Gwangju 61005, Korea
Full list of author information is available at the end of the article

groups who could provide detailed symmetry information of tetragonal-like and rhombohedral-like phases, but it should be noted that most of the works have been done with assumptions of the homogeneous and coherent contributions of constituent domains [18, 19].

In this paper, we demonstrate that the distribution and characteristics of ferroelectric domains for the tetragonal-like $BiFeO_3$ (T-BFO) can be investigated by using a conventional SHG microscope with proper adjustments of probe beam sizes with respect to the domain size. Since this T-BFO hosts nanometer-sized domains which form specific patterns of micrometer-sized domains, it provides an excellent environment to address how the SHG responses are contributed to by each ferroelectric domain of different sizes and their mixtures. We mapped the sample with a probe beam of several sizes and found large position-dependent variations of the SHG signal which originate from distinct characteristics of the domain distribution. By considering the coherent and incoherent contributions of each domain to the SHG response, we could successfully explain such experimental results. We therefore expect that symmetry information of the individual nanometer-sized domain can be obtained even from the far-field microscopic measurement provided that the proper modeling can be chosen and applied between the incoherent and the coherent approaches.

Methods

The T-$BiFeO_3$ thin film is grown on a $LaAlO_3$ (001) substrate by using a pulsed laser deposition technique of which details can be found elsewhere [4]. The thickness of T-BFO film is about 30 nm. For the SHG experiment, fundamental light of 800 nm wavelength illuminates the sample in a normal incidence, and second harmonic light is detected in reflection geometry. We used laser pulses from the Ti:sapphire laser system for fundamental light which has a pulse width of about 30 fs and a repetition rate of 80 MHz. It has a power of about 20 mW and is focused down to the diffraction limit using an objective lens with a magnification of ×50 and a 0.75 numerical aperture. Polarization states of fundamental and second harmonic light are set to be parallel (XX) or orthogonal (XY) as shown in Fig. 1a.

Results and discussion

We first monitored a distribution of the ferroelectric domains by using a scanning probe microscope (Bruker, MultiMode-V). PFM measurements were performed at a scan rate of 3 μm/s using Pt-coated Si conductive tips (MikroMasch, NSC35) with applying an ac driving voltage of 3 V_{pp} at a frequency of 12 kHz. Figure 1a displays the PFM image of T-BFO obtained at room temperature. It shows that ferroelectric domains form stripe patterns in a submicron length scale and the larger micron-scale areas are distributed with typical stripe orientations along 45° or 135°. In Fig. 1c, we schematically draw four types of such domain patterns. Owing to the monoclinic distortion, T-BFO has an in-plane component of the polarization as well as the polarization along the *c*-axis [7]. As the normal incidence in SHG measurement, a configuration adopted in this work is not sensitive to the out-of-plane polarization component; we here restrict our interest only in the in-plane component. We consider first a nanometer-sized domain with a polarization along the *a*- or *b*-axis, and their head-to-tail combination with a domain wall formed along the diagonal directions. Consistently with the PFM result, we hence consider four possible combinations of such domains as depicted in Fig. 1c. It should be noted that each stripe pattern is distributed over a few micrometers or even tens of micrometer scales as shown in Fig. 1a.

Before showing the experimental result, let us discuss the SHG response simulations of T-BFO (C_{1h} point group) with a consideration of each domain configuration [20]. Intensity of second harmonic (SH) light $I(2\omega)$ is given in proportion to the induced SH polarization $P(2\omega)$ as $I(2\omega) \propto |P(2\omega)|^2 = |\chi_{ijk}E_jE_k|^2$, where χ_{ijk} represents the nonlinear susceptibility of the material, E_i is the electric field component of the fundamental light, and i, j, and k denote the crystallographic axes. The transverse coherence length L_T is determined as $L_T = \lambda R/2D$ [21]. Here, D is a size of the domain which acts as an SH light source and λ is a wavelength of SH light, i.e., 400 nm. R denotes a distance (0.38 mm) from the sample surface to the objective lens. Note that the coherence length is comparable to the objective lens size (625 μm in its diameter) when D is about 100 nm. Therefore, when we consider the contributions of multi-domains to the SHG, it is reasonable to assume that each nanometer-sized domain having a size of about 50 nm contributes to the SHG responses coherently as $I(2\omega) \propto (P_1 + P_2)^2$, whereas micro-domains contribute to $I(2\omega)$ incoherently as $I(2\omega) = P_1^2 + P_2^2$. Here, P_1 and P_2 imply the induced SH polarizations of each nano- or micro-domain when only two types of domains are considered.

Figure 1d shows the azimuth-dependent $I(2\omega)$ obtained by considering such coherent and incoherent contributions of different domains. For the leftmost case, we consider the coherent summation of two nanometer-sized domains corresponding to the first configuration listed in Fig. 1c. The polarization direction of each nanometer-sized single domain is along the *x*- and *y*-axes. We take $\chi_{xxx} = 0.35$, $\chi_{xyy} = 1.0$, and $\chi_{yxy} = 0.4$ for the domain with the *x*-axis polarization and $\chi_{yyy} = -0.35$, $\chi_{yxx} = -1.0$, and $\chi_{xyx} = -0.4$ for the domain with the *y*-axis polarization. All other susceptibility components are assumed to be zero. For the rightmost case, we consider the fourth configuration of Fig. 1c with the same values

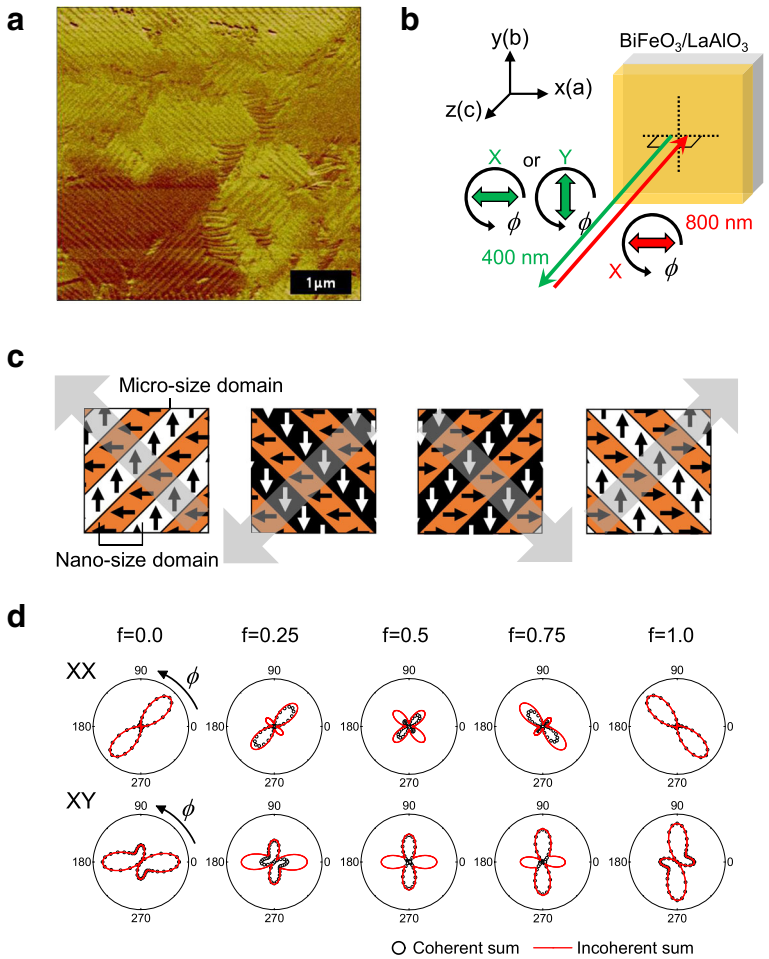

Fig. 1 Ferroelectric domain distribution in a tetragonal $BiFeO_3$ film and expected second harmonic generation results as coherent and incoherent contributions of multi-domains. **a** Piezoelectric force microscope image. *Stripe-patterned* domains are seen with two distinct orientations. **b** Schematic description of the second harmonic generation experiment. **c** Four types of *stripe patterns* of ferroelectric domains. **d** Polar plots of simulated second harmonic responses depending on a portion of different domains. Both coherent and incoherent summations are presented

of χ_{xxx}, χ_{xyy}, and χ_{yxy} with changes in the sign of χ_{yyy}, χ_{yxx}, and χ_{xyx}. The azimuth-dependent $I(2\omega)$ for the former and latter cases are displayed in the first and fifth plots in Fig. 1d; the XX response in each configuration has maximum values along the direction perpendicular to the net polarization axis because $|\chi_{xxx}| < |\chi_{xyy}|$ and $|\chi_{yyy}| < |\chi_{yxx}|$. With these two cases as end members, we consider coherent and incoherent summations with different portions f ($0.0 < f < 1.0$) or $1\text{-}f$ of the contribution from each end member. In the intermediate cases with $f = 0.75$, 0.5, and 0.25, the incoherent summation leads to the finite value of the minimum $I(2\omega)$ and more swollen lobe shape compared to the coherent summation.

From now on, we present the experimental SHG results and discuss them based on the coherent and incoherent analyses of the multi-domain contribution. Before each SHG measurement, we characterized the beam size of fundamental light at the sample position using a knife-edge method [22]. Figure 2a shows an intensity (open symbols) obtained with a displacement of the knife edge by 1 μm. We fit the results assuming the Gaussian distribution of the beam intensity and estimate the beam size W, a width defined by two points having the $1/e^2$ intensity of the maximum value as 0.7, 1.5, 2.1, and 3.9 μm.

Figure 2b displays a two-dimensional distribution of $I(2\omega)$ obtained with $W = 0.7$ μm. The displacement for each step is 1 μm, and the mapping area is 25×25 μm^2. The sample azimuth Φ is fixed as 45° in the XX geometry. $I(2\omega)$ exhibits a large variation with no discernible pattern. These results clearly indicate that the domain size in the probed area is comparable to the beam size.

We can get a deeper insight into the ferroelectric domain by examining the azimuth-dependent of $I(2\omega)$ at each sample position. Figure 2c displays the results

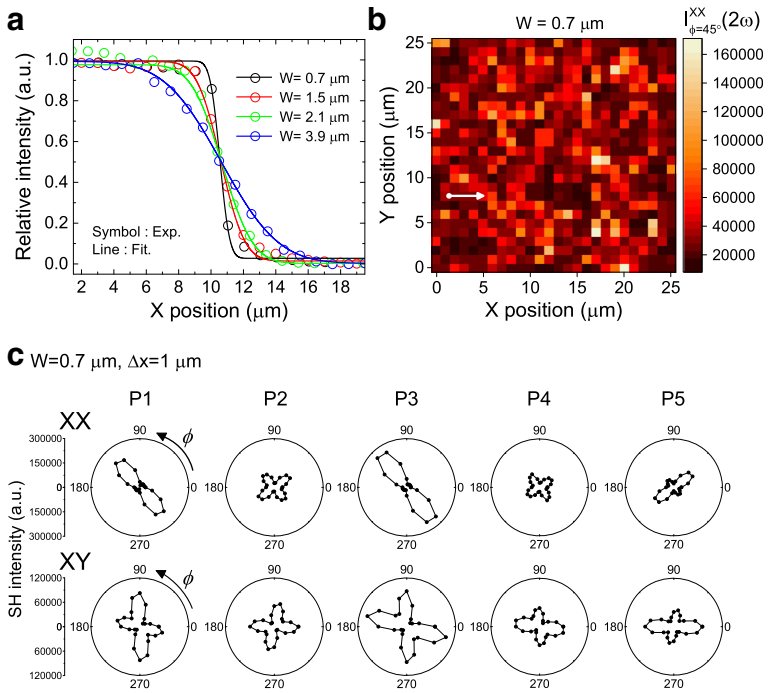

Fig. 2 Second harmonic generation (SHG) results obtained with a beam size of 0.7 μm. **a** Knife-edge experimental results to characterize the beam size. **b** The SHG intensity mapping image obtained with a beam size 0.7 μm over the area of 25 × 25 μm^2. **c** Azimuth-dependent polar plots of the SHG intensity obtained at different sample positions along the *arrow* in **b**

obtained at five representative positions. Although each point is displaced by 1 μm from neighboring points, the SHG results vary quite drastically from a point to a point. Looking at the results of the XX geometry, although P_1, P_3, and P_5 exhibit twofold symmetry, P_2 and P_4 show a fourfold symmetry. The behaviors in the XY geometry are relatively less distinct. Nevertheless, P_1 and P_3 have a main lobe at $\Phi = 135°$ (315°); P_5 has the corresponding maximum at 45° (225°). These results strongly suggest that each measured point has distinct preferred planar orientations of the ferroelectric polarization. Actually, the patterns of the experimental result can be identified by the simulation results shown in Fig. 1d; P_1 (P_3) and P_5 correspond to the case $f = 1.0$ and 0.0, respectively. Also, P_2 and P_4 can be identified as the case $f = 0.5$ (incoherent). In other words, the results of P_1 and P_5 pick up the single configuration of four possible micro-domains shown in Fig. 1c, and the measurement at P_2 and P_4 covers two (or more) micro-domains. Considering the coherence length, it is expected that such micro-domains contribute to the SHG response incoherently. From these results, we therefore confirm that nano-domains compose a single micro-domain and contribute to the SH response coherently, whereas micro-domains contribute to the SHG response incoherently. Furthermore, the part of symmetry information of a single nano-sized domain can be obtained from the analysis of the single micro-domain contribution; the simulation results in Fig. 1 give that $\chi_{xxx} = 0.35$, $\chi_{xyy} = 1.0$, and $\chi_{yxy} = 0.4$ for the nano-domain with the x-axis polarization. (In the XY geometry, the relative intensity at $\Phi = 45°$ and 135° appears oppositely to the simulation results in Fig. 1d. This discrepancy requires further analysis.)

We increased the beam size and monitored how the SHG response varies depending on it. Figure 3a, b show the results of the two-dimensional mapping obtained with $W = 1.5$ and 2.1 μm, respectively. Here, the interval between two neighboring points is kept as the same, i.e., $\Delta x = 1$ μm, and the power of fundamental light is also maintained. As the beam size increases from $W =$ 0.7 to 1.5 and to 2.1 μm, $I(2\omega)$ decreases as expected from the smaller beam fluence. Also, the distribution of $I(2\omega)$ becomes to have a less position dependence.

Azimuth-dependent SHG patterns also show systematic variations as the beam size increases. For $W =$ 1.5 μm, we can still observe the strong position dependence; P_1 and P_4 reflect two distinct micro-domains, and the other points can be considered as mixtures of such micro-domains. Compared with the results for $W = 0.7$ μm, it is clear that the incoherent contributions become more discernible for $W = 1.5$ μm; the minimum value of the SHG intensity becomes non-zero, and it is much larger than for $W = 0.7$ μm. For W

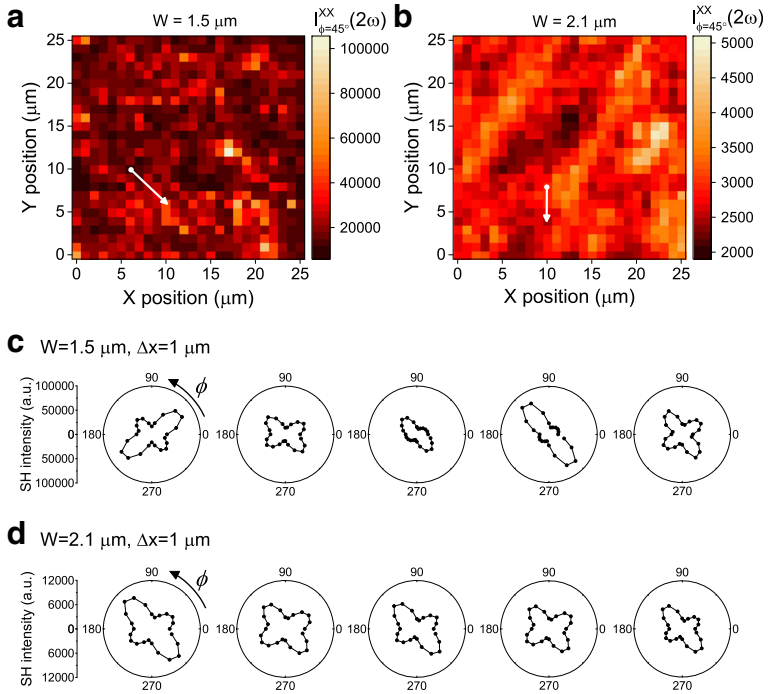

Fig. 3 Second harmonic generation (SHG) results obtained with beam sizes of 1.5 and 2.1 μm. **a**, **b** The SHG intensity mapping image obtained with beam sizes of 1.5 and 2.1 μm, respectively. **c**, **d** Azimuth-dependent polar plots of the SHG intensity obtained at different sample positions with beam sizes of 1.5 and 2.1 μm, respectively, along the *arrows* in each figure

= 2.1 μm, such tendency becomes more pronounced; there is almost no position dependence as shown in Fig. 3d. This is probably due to the influence of the dominance of a single micro-domain over the entire probing area. With $W = 0.7$ μm, a single micro-domain can be probed, and hence, the SHG intensity is determined by the coherent contribution from the constituent nano-sized domains. With $W = 1.5$ μm and 2.1 μm, on the other hand, several micro-domains are probed together, and they contribute to the SHG intensity as an incoherent summation.

As a final test, we further increased the probe beam size up to $W = 3.9$ μm of which result is displayed as closed circles in Fig. 4. Also shown are the results for smaller Ws which are averaged over several points around the beam central position for $W = 3.9$ μm. Interestingly, such averaged results for $W = 0.7$, 1.5, and 2.1 μm appear quite similarly in both XX and XY geometry with the single measurement results for $W = 3.9$ μm. As this average process of the measured SH intensity is identical to the incoherent summation of each micro-domain contribution, this agreement confirms our understanding of the incoherent contribution to the SHG responses of multi-micro-domains.

Conclusions

We investigated the ferroelectric domains of a tetragonal $BiFeO_3$ film by using a second harmonic generation (SHG) technique. Whereas the normal incidence SHG measurement provides us with clear information about the in-plane component of the ferroelectric polarization, we found large variations of the SHG responses from a point to a point of the sample. This clearly indicates the inhomogeneity of the domain distribution. By reducing the beam size down to 0.7 μm, we demonstrated that the observed SHG results could reveal the symmetry characteristic of individual micrometer-sized domains which is determined by types of constituent nanometer-sized

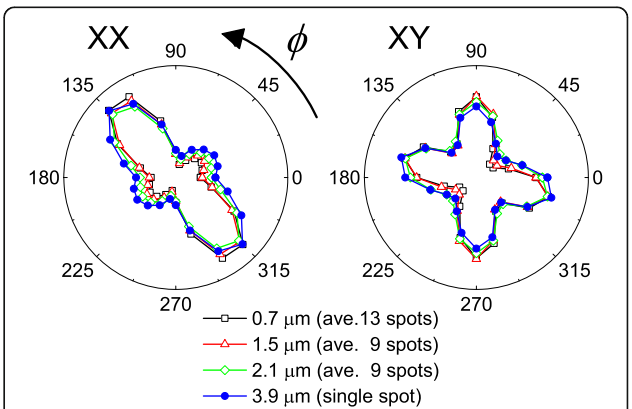

Fig. 4 Second harmonic generation (SHG) results obtained with a beam size of 3.9 μm. Also shown are the three other curves for the different beam sizes which are obtained as averages over several points

domains. By increasing the beam size up to 3.9 μm, we found the SHG response with a much less position dependence. Actually, we could reproduce this SHG result obtained with a 3.9 μm beam size with averages of several results obtained with smaller beam sizes and confirmed that each micro-domain contributes to the SHG responses incoherently. Therefore, we can have a chance to retrieve symmetry information of the individual nanometer-sized or even micrometer-sized domain if we can apply a proper model between coherent and incoherent analysis of the SHG results.

Abbreviations

BFO: BiFeO3; PFM: Piezoresponse force microscopy; SH: Second harmonic; SHG: Second harmonic generation; T-BFO: Tetragonal $BiFeO_3$; XX: Parallel; XY: Orthogonal

Acknowledgements

We acknowledge Y. G. Choi for the technical support in performing the second harmonic measurements. This work was supported in part by the Basic Science Research Program through the National Research Foundation of Korea (NRF) funded by the Ministry of Science, ICT and Future Planning (Nos. 2015R1A5A1009962, 2015R1A1A1A05001560). The work at KAIST was supported by the NRF via the Center for Quantum Coherence in Condensed Matter (2016R1A5A1008184).

Authors' contributions

CJR and SYH carried out the second harmonic generation experiment and analyzed the results. CSW, KEK, and CHY prepared the $BiFeO_3$ thin films and carried out the piezoelectric force microscope experiment. CJR and JSL wrote the manuscript. JSL supervised the research. All authors read and approved the final manuscript.

Competing interests

The authors declare that they have no competing interests.

Publisher's Note

Author details

[1]Department of Physics and Photon Science, Gwangju Institute of Science and Technology (GIST), 123 Cheomdangwagi-ro, Buk-gu, Gwangju 61005, Korea. [2]Department of Physics, Korea Advanced Institute of Science and Technology (KAIST), 291 Daehak-ro, Yuseong-gu, Daejeon 305-701, Korea.

Received: 2 February 2017 Accepted: 4 May 2017
Published online: 15 May 2017

References

1. Roginska YE, Tomashpo YY, Venevtse YN, Petrov VM, Zhdanov GS (1966) Nature of dielectric and magnetic properties of $BiFeO_3$. Sov Phys JETP 23:47
2. Sosnowska I, Loewenhaupt M, David WIF, Ibberson RM (1992) Investigation of the unusual magnetic spiral arrangement in $BiFeO_3$. Physica B 180–181:117
3. Wang J, Neaton JB, Zheng H, Nagarajan V, Ogale SB, Liu B, Viehland D, Vaithyanathan V, Schlom DG, Waghmare UV, Spaldin NA, Rabe KM, Wuttig M, Ramesh R (2003) Epitaxial $BiFeO_3$ multiferroic thin film heterostructures. Science 299:1719
4. Ko KT, Jung MH, He Q, Lee JH, Woo CS, Chu KH, Seidel J, Jeon BG, Oh YS, Kim KH, Liang WI, Chen HJ, Chu YH, Jeong YH, Ramesh R, Park JH, Yang CH (2011) Concurrent transition of ferroelectric and magnetic ordering near room temperature. Nat Commun 2:567.
5. Chu YH, Martin LW, Holcomb MB, Gajek M, Han SJ, He Q, Balke N, Yang CH, Lee D, Hu W, Zhan Q, Yang PL, Fraile-Rodriguez A, Scholl A, Wang SX, Ramesh R (2008) Electric-field control of local ferromagnetism using a magnetoelectric multiferroic. Nat Mater 7:478.
6. Zhao T, Scholl A, Zavaliche F, Lee K, Barry M, Doran A, Cruz MP, Chu YH, Ederer C, Spaldin NA, Das RR, Kim DM, Baek SH, Eom CB, Ramesh R (2006) Electric control of antiferromagnetic domains in multiferroic $BiFeO_3$ films at room temperature. Nat Mater 5:823
7. Chen Z, Luo Z, Huang C, Qi Y, Yang P, Lu Y, Hu C, Wu T, Wang J, Gao C, Sritharan T, Chen L (2011) Low-symmetry monoclinic phases and polarization rotation path mediated by epitaxial strain in multiferroic $BiFeO_3$ thin films. Adv Funct Mater 21:133
8. Zeches RJ, Rossell MD, Zhang JX, Hatt AJ, He Q, Yang C-H, Kumar A, Wang CH, Melville A, Adamo C, Sheng G, Chu Y-H, Ihlefeld JF, Erni R, Ederer C, Gopalan V, Chen LQ, Schlom DG, Spaldin NA, Martin LW, Ramesh R (2009) A strain-driven morphotropic phase boundary in $BiFeO_3$. Science 326:977
9. Christen HM, Nam JH, Kim HS, Hatt AJ, Spaldin NA (2011) Stress-induced R-M_A-M_C-T symmetry changes in $BiFeO_3$ films. Phys Rev B 83:144107
10. Lummen TTA, Gu Y, Wang J, Lei S, Xue F, Kumar A, Barnes AT, Barnes E, Denev S, Belianinov A, Holt M, Morozovska AN, Kalinin SV, Chen LQ, Gopalan V (2014) Thermotropic phase boundaries in classic ferroelectrics. Nat Commun 5:3172.
11. Sharan A, Lettieri J, Jia Y, Tian W, Pan X, Schlom DG, Gopalan V (2014) Bismuth manganite: a multiferroic with a large nonlinear optical response. Phys Rev B 69:214109.
12. Yokota H, Haumont R, Kiat JM, Matsuura H, Uesu Y (2009) Second harmonic generation microscopic observations of a multiferroic $BiFeO_3$ single crystal. Appl Phys Lett 95:082904
13. Barad V, Lettieri J, Theis CD, Schlom DG, Gopalan V, Jiang JC, Pan XQ (2001) Probing domain microstructure in ferroelectric $Bi_4Ti_3O_{12}$ thin films by optical second harmonic generation. J Appl Phys 89:1387
14. Wang J, Jin K, Guo H, Gu J, Wan Q, He X, Li X, Xu X, Yang G (2016) Evolution of structural distortion in $BiFeO_3$ thin films probed by second harmonic generation. Sci Rep 6:38268
15. Hamh SY, Park S-H, Jerng S-K, Jeon JH, Chun SH, Jeon JH, Kahng SJ, Yu K, Choi EJ, Kim S, Choi S-H, Bansal N, Oh S, Joonbum P, Byung-Woo K, Jun Sung K, Lee JS (2016) Surface and interface states of Bi_2Se_3 thin films investigated by optical second-harmonic generation and terahertz emission. Appl Phys Lett 108:051609
16. Neacsu CC, Van Aken BB, Fiebig M, Raschke MB (2013) Second-harmonic near-field imaging of ferroelectric domain structure of $YMnO_3$. Phys Rev B 79:100107(R)
17. Sänger I, Pavlov VV, Bayer M, Fiebig M (2006) Distribution of antiferromagnetic spin and twin domains in NiO. Phys Rev B 74:144401
18. Trassin M, De Luca G, Manz S, Fiebig M (2015) Probing ferroelectric domain engineering in $BiFeO_3$ tin films by second harmonic generation. Adv Mater 27:4871
19. Lofland SE, McDonald KF, Metting CJ, Knoesel E, Murakami M, Aronova MA, Fujino S, Wutting M, Takeuchi I (2006) Epitaxy, texturing, and second-harmonic generation in $BiFeO_3$ thin films. Phys Rev B 73:092408
20. Nonlinear optics, edited by Robert W. Boyd. (Academic press, lic, 2008), Chaps. I.
21. Elements of modern X-ray physics, edited by Jens AN, and MacMorrow DF. (Wiley, 2010), Chaps. I.
22. De Araujo MAC, Silva R, De Lima E, Pereira DP, De Oliveira PC (2009) Measurement of Gaussian laser beam radius using the knife-edge technique: improvement on data analysis. Appl Opt 48:393